

1  
2

# Final manuscript version of

Tectonophysics 792 (2020) 228588



Contents lists available at ScienceDirect

Tectonophysics

journal homepage: [www.elsevier.com/locate/tecto](http://www.elsevier.com/locate/tecto)



## A new tectonic map of the Iranian plateau based on aeromagnetic identification of magmatic arcs and ophiolite belts



Vahid Teknik<sup>a,b,c,\*</sup>, Hans Thybo<sup>a,d</sup>, Irina M. Artemieva<sup>e,f</sup>, Abdolreza Ghods<sup>c</sup>

<sup>a</sup> Eurasia Institute of Earth Sciences, Istanbul Technical University, Istanbul, Turkey

<sup>b</sup> Department of Geosciences and Natural Resource Management, University of Copenhagen, Copenhagen, Denmark

<sup>c</sup> Institute for Advanced Studies in Basic Sciences, Zanjan, Iran

<sup>d</sup> Centre for Earth Evolution and Dynamics, University of Oslo, Oslo, Norway

<sup>e</sup> Department of Geophysics, Stanford University, Stanford, CA, USA

<sup>f</sup> Section of Marine Dynamics, GEOMAR Helmholtz Center for Ocean Research, Kiel, Germany

3  
4

\* Corresponding author at: Eurasia Institute of Earth Sciences, Istanbul Technical University, Istanbul, Turkey.  
E-mail address: [vahid.teknik@gmail.com](mailto:vahid.teknik@gmail.com) (V. Teknik).

<https://doi.org/10.1016/j.tecto.2020.228588>

Received 11 October 2019; Received in revised form 27 July 2020; Accepted 8 August 2020

Available online 13 August 2020

0040-1951/ © 2020 Elsevier B.V. All rights reserved.

5  
6

7

8

## A new tectonic map of the Iranian plateau based on aeromagnetic

9

## identification of magmatic arcs and ophiolite belts

10 Vahid Teknik (1,2,3)\*, Hans Thybo (1,4), Irina M. Artemieva (5,6), Abdolreza Ghods(3)

11 (1) Eurasia Institute of Earth Sciences, Istanbul Technical University, Istanbul, Turkey (2)Department of  
12 Geosciences and Natural Resource Management, University of Copenhagen, Copenhagen, Denmark , (3) Institute  
13 for Advanced Studies in Basic Sciences, Zanjan, Iran. (4) Centre for Earth Evolution and Dynamics, University of  
14 Oslo, Oslo, Norway (5) Department of Geophysics, Stanford University, Stanford, CA, USA (6) Section of Marine  
15 Dynamics, GEOMAR Helmholtz Center for Ocean Research, Kiel, Germany.

16 • Corresponding author email: [vahid.teknik@gmail.com](mailto:vahid.teknik@gmail.com)

17

18 Highlights:

- 19 • The Radially averaged power spectrum method is applied to calculate average magnetic  
20 susceptibility in Iran.
- 21 • The shows known occurrences of Magmatic-Ophiolite Arcs (MOA) correlate with high average  
22 susceptibility areas.
- 23 • We interpret two parallel, hitherto unknown, MOAs in eastern Iran developed in a steeply  
24 dipping (>60° dip) subduction zone.
- 25 • Neo-Tethys subduction shallow angle (<20°) in NW and steep (>60°) in SE of Urmia-Dokhtar  
26 Magmatic Arc indicates slab tearing.
- 27 • We define a new outline of the economically important Tabas sedimentary basin.

28

29

### 30 Abstract

31 The Iranian plateau is one of the most complex geodynamic settings within the Alpine-Himalayan  
32 belt. The Paleo-Tethys and Neo-Tethys ocean subduction is responsible for the formation of several  
33 magmatic arcs and sedimentary basins within the plateau. These zones mostly are separated by  
34 thrust faults related to paleo-suture zones, which are highlighted by ophiolites. Sediment cover and  
35 overprint of a different magmatic phase from late Triassic to the Quaternary impede identification  
36 of some magmatic arcs and ophiolite belts.

37 We track the known magmatic arcs, such as the Urmia-Dokhtar Magmatic Arc (UDMA), and  
38 unknown, sediment covered magmatic arcs by aeromagnetic data. We present a new map of  
39 average susceptibility calculated by the radially averaged power spectrum method. High average  
40 susceptibility values indicate the presence of a number of lineaments that correlate with known  
41 occurrences of Magmatic-Ophiolite Arcs (MOA), and low average susceptibility coincides with  
42 known sedimentary basins like Zagros, Makran, Kopeh-Dagh, and Tabas. In analogy to Zagros,  
43 low average susceptibility values indicate sedimentary basins to the south of the Darouneh fault  
44 and in the northern part of the Lut, Tabas and Yazd blocks. We interpret the Tabas basin as a pull-  
45 apart or back-arc basin. We identify hitherto unknown parallel MOAs in eastern Iran and the SE  
46 part of UDMA which both indicate steeply dipping ( $>60^\circ$  dip) paleo-subduction zones. In contrast,  
47 we interpret shallow subduction ( $<20^\circ$  dip) of Neo-Tethys in the NW part of UDMA as well as in  
48 the Sabzevar-Kavir MOA.

49 **Keywords:** Aeromagnetic data, susceptibility, Tectonics, Iranian plateau, magmatic arcs,  
50 ophiolites, sedimentary basins.

## 51 1. Introduction

52 The Iranian Plateau is a complex puzzle of continental and oceanic fragments that were  
53 amalgamated during the closure of the Paleo-Tethys and Neo-Tethys oceans. The structure of the  
54 plateau reflects the geological-tectonic evolution, including subduction, collision, and  
55 magmatism in the Alpine–Himalayan orogenic belt (Stampfli and Borel, 2002) (**Figure 1**). The  
56 opening and continuous subduction along the northern margin of the Paleo-Tethys ocean from  
57 Paleozoic to late Triassic, and later along the northern margin of the Neo-Tethys ocean from  
58 Mesozoic to Cenozoic time, emplaced several ophiolite belts and long magmatic arcs, and also

59 created intracontinental basins (Berberian and King, 1981; Richards, 2015; Stampfli and Borel,  
60 2002; Verdel et al., 2011). Ophiolites are normally emplaced along major faults and are generally  
61 interpreted as marks of sutures. The vast plateau area includes remote parts, which are sparsely  
62 studied and mostly covered by young and thick sedimentary sequences. Almost no information  
63 on basement age is available in these regions with the exception of some Precambrian age  
64 continental fragments trapped within the Iranian Plateau.

65 Interpretation of aeromagnetic data provides an efficient and fast geophysical tool for geological  
66 mapping of vast areas as the Iranian plateau. The highest magnetic susceptibility values are  
67 usually observed in igneous rocks and ophiolites in contrast to the low values in most  
68 sedimentary rocks (Clark and Emerson, 1991; Hunt et al., 1995; Teknik et al., 2019) (**Figure 2**).

69 The radially averaged power spectrum (RAPS) method (e.g. Bouligand et al., 2009; Maus and  
70 Dimri, 1995) is widely used for estimating the Curie depth. Here we extend its application to  
71 calculation of the vertically averaged crustal magnetic susceptibility from aeromagnetic data.

72 Application of this method provides a solution which is insensitive to the latitude dependence of  
73 magnetic data (Maus and Dimri, 1995a), and therefore provides a tool for estimation of the  
74 horizontal variation of susceptibility and for identification of high susceptibility rocks in  
75 magmatic and suture zones. This routine is easy to implement and fast in comparison to  
76 traditional inversion methods, which are based on further assumptions and require a priori  
77 information for calculation of the vertical variation of susceptibility (e.g. Li and Oldenburg,  
78 1993).

79 In this work, we use the RAPS method to calculate the average crustal susceptibility in the  
80 Iranian plateau. The results indicate qualitative correlation between strong susceptibility  
81 anomalies and the distribution of magmatic arcs and ophiolite belts. Low susceptibility values

82 coincide with major sedimentary basins where the geology is known. On this basis, we extend  
83 our analysis to mapping similar features in the remote and sediment-covered parts of the Iranian  
84 Plateau. Our analysis identifies unknown magmatic ophiolite arcs (MOA) and boundaries of  
85 sedimentary basins, and thereby we revise parts of the tectono-magmatic evolution of the Iranian  
86 Plateau.

## 87 2. **Geologic setting**

88 The geodynamic evolution of the Iranian Plateau has been controlled by the opening and closure  
89 of the Neo-Tethys and Paleo-Tethys oceans in the south and north of the Iranian plateau,  
90 respectively (Stampfli and Borel, 2002). During Permian extension of the Neo-Tethys Ocean,  
91 various continental blocks (Cimmerian blocks) were rifted off from the NE margin of Gondwana  
92 while the Paleo-Tethys Ocean subducted beneath Laurasia (Richards, 2015; Stampfli and Borel,  
93 2002). These blocks, including central Iranian blocks collided with Laurasia during the closure of  
94 the Paleo-Tethys ocean and the subsequent Cimmerian orogeny. After the eventual collision of  
95 the Central Iranian blocks with Laurasia, the subduction shifted SW-ward, and Neo-Tethys  
96 subducted beneath the Central Iranian blocks in the Triassic (Stampfli and Borel, 2002). The  
97 subduction of the Tethys oceans and consequent collision formed a series of magmatic arcs and  
98 back-arc basins (the largest may be the south Caspian basin and parts of the Black Sea).  
99 Eventually, the Neo-Tethys Ocean and smaller back arc basins were closed by the collision of the  
100 Arabian plate with central Iranian blocks in the early Miocene. Trapped remnants of the Tethys  
101 Oceans are mapped as ophiolites within the collisional belt (Berberian and King, 1981; Boulin,  
102 1991; Nowroozi, 1971; Stocklin, 1968; Verdel et al., 2011)

103 Three major structural units of the Iranian plateau are categorized by reconstruction of the Paleo-  
104 Tethys and Neo-Tethys oceans (Berberian and King, 1981): (1) The Zagros - Makran orogenic  
105 system, which formed during subduction of Neo-Thetys and subsequent collision; (2) The  
106 Central Iranian micro plate which formed by amalgamation of Cimmerian blocks to Eurasia; and  
107 (3) The NE Turan part of the Iranian Plateau, which formed in relation to the subduction of  
108 Paleo-Thetys and subsequent collision (**Figure 1**).

109 The NW-SE to E-W trending Zagros-Makran orogenic belt is located in the western and  
110 southern parts of the Iranian plateau. The Talesh-Alborz-Kopeh-Dagh belt in the northern part of  
111 the Iranian plateau trends along the southern edge of Eurasia and the south Caspian basin. The  
112 Central Iranian micro plates and magmatic arcs are located between these two major orogenic  
113 belts. Zagros, Makran, Kopeh-Dagh, eastern Alborz and some central Iranian blocks, e.g. Tabas,  
114 include major sedimentary basins, which host hydrocarbon reservoirs. The Sanandaj-Sirjan  
115 metamorphic Zone (SSZ), and the parallel Urmia-Dokhtar Magmatic Arc (UDMA), extend from  
116 the NW to the SE of the plateau. The Sabzevar-Kavir magmatic ophiolite belt and the eastern  
117 magmatic zone are located at the boundaries of the Central Iranian micro plates and in the  
118 eastern Sistan suture Zone (**Figure 1 and 3a**).

119 **Urumieh-Dokhtar Magmatic Arc (UDMA) evolution:** The Urumieh-Dokhtar Magmatic Arc  
120 formed by subduction of the Neo-Tethys Ocean beneath Central Iran (e.g. Berberian and King,  
121 1981; Verdel et al., 2011). Different phase of magmatic activity may have overlapped in the  
122 Iranian plateau. The magmatic activity related to the Neo-Tethys subduction started from Jurassic  
123 (155 MA), in the SSZ Mesozoic arc. After a magmatic activity gap in the early Cretaceous,  
124 magmatic activity started along the UDMA from Late Cretaceous (100MA), but the maximum  
125 magmatic activity of the UDMA elongated an igneous “flare-up” event during the Eocene-

126 Oligocene (55–25 Ma) (**Figure 3b**). The UDMA magmatism ceased in the Late Miocene. Then,  
127 the post-collisional volcanism started ca. 11 Ma in the Lesser Caucasus, NW Iran and eastern  
128 Anatolia regions (**Figure 3b**) (Chiu and et. al., 2013).

129 **Zagros and Makran orogenic belt:** The NW-SE trending Zagros orogenic system can be  
130 divided into three parallel structural domains (a) Zagros Fold and thrust belt (ZFTB); (b) The  
131 Mesozoic metamorphic and magmatic Sanandaj–Sirjan Zone separated from ZFTB by the Main  
132 Recent Fault (MRF) and Main Zagros Thrust (MZT), and (c) the Tertiary Urumieh–Dokhtar  
133 Magmatic Arc (Berberian, 1995; Sepehr and Cosgrove, 2004) (**Figure 1**). Its SE continuation  
134 identifies the location where the last remnant of the Neo-Tethys Ocean is currently subducting  
135 along the Makran trench south of Iran and Pakistan. North of this belt, the Cenozoic Jazmurian  
136 basin is interpreted as a back-arc basin of the Makran subduction system (Burg, 2018; Glennie et  
137 al., 1990; McCall and Kidd, 1982).

138 **Central Iran microplates:** The region includes three major crustal blocks (from east to west):  
139 the Lut, Tabas, and Yazd blocks (**Figure 1**). Geological origin and age of this continental part  
140 are poorly known but the blocks are considered Cimmerian (Richards, 2015; Stampfli and Borel,  
141 2002). The presence of ophiolite belts across central Iran suggests that several small back-arc  
142 basins formed during the subduction of the Neo-Tethys Ocean. These inner plateau oceans (such  
143 as Sabzevar and Sistan oceans) were destroyed mainly after the collision between the Arabian  
144 plate and central Iranian plates in the Neogene (Şengör, 1990a; Şengör 1990b). The Sabzevar-  
145 Kavir magmatic ophiolite arc (MOA), which includes an ophiolitic *mélange*, is considered one of  
146 the back-arc basins (Richards, 2015).

147 **Eastern Iran:** The Sistan zone - Lut region includes ophiolites, Tertiary magmatic rocks, and  
148 major, late Tertiary strike-slip faults. No comprehensive tectonic – geological mapping has been  
149 carried out since the mapping by Stocklin (1968). Key questions concern the location of the  
150 eastern boundary of the Central Iranian block and the nature of obducted ophiolites and their  
151 relationship to the Sabzevar-Kavir zone. Back-arc rifting may have opened several small oceanic  
152 basins and subsequent closure caused magmatism in the eastern Iran (Alaminia et al., 2013;  
153 Arjmandzadeh et al., 2011; Richards, 2015).

154 **Talesh-Alborz and Kopeh-Dagh:** The arch-curved, 3-5 km high Alborz Mountains south of the  
155 Palaeo-Tethys suture zone includes about 5 km of Phanerozoic rocks (Ballato et al., 2011; Teknik  
156 and Ghods, 2017). The Kopeh-Dagh Mountains mark the north-eastern edge of the Arabia–  
157 Eurasia collision zone in Iran and include a 10 km deep sedimentary basin with folded  
158 Mesozoic-Tertiary sedimentary rocks (Berberian and Berberian, 1981).

159 **South Caspian Basin** includes a 20–25 km thick sedimentary sequence on top of a 10 km thick  
160 crystalline crust (Jackson et al., 2002) . Its origin is disputed. Models include a Paleo-Tethys  
161 oceanic remnant (Dewey et al., 1973), a trapped remnant of an early Mesozoic back-arc oceanic  
162 crust (Berberian, 1983), and a Cretaceous to Paleogene strike slip-related pull-apart basin  
163 (Şengör, 1990). Our recent gravity modelling indicates that the South Caspian Basin may be of  
164 continental rather than oceanic origin (Teknik et al., 2019).

### 165 **3. Data and Method**

166 We apply the radially averaged power spectrum (RAPS) method to calculate the average crustal  
167 magnetic susceptibility. This approach assumes fractal induced crustal magnetization and parallel  
168 or antiparallel remanent magnetization to the present geomagnetic field (Maus et al., 1997). The



169 susceptibility is estimated inside a horizontal window and we assume that the values represent  
170 the vertically averaged susceptibility from the surface to the Curie depth point (CDP) inside the  
171 window. The spatial resolution is limited by the averaging window (80 x 80 km) with 90%  
172 overlap between windows.

173 The magnetic data originates from the aeromagnetic survey of Iran, which was conducted by  
174 Aeroservice (Houston, Texas) in 1974-1977 for the Iranian Geological Survey with an average  
175 line spacing of 7.5 km and perpendicular lines every 40 km. The survey includes more than  
176 250,000 km profiles with ca. 4.4 million data points. The direction of flight lines varies and  
177 depends on the topographical and geological features trend. We use the composite aeromagnetic  
178  $1 \times 1$  km grid calculated from the original raw data by Saleh, (2006) by using bidirectional  
179 interpolation scheme (**Figure 4**).

#### 180 **4. Results**

181 **Sedimentary basins:** Sedimentary rocks usually are weakly magnetized and we mainly attribute  
182 low average susceptibility to the presence of sedimentary basins. Our results confirm the location  
183 of major basins, such as in the Zagros, Kopeh-Dagh and Makran accretionary prisms with their  
184 extremely low average susceptibility. Similar to these basins, we suggest considerable sediment  
185 cover without any magmatic activity in the Tabas basin and central part of the Yazd block. The  
186 low susceptibility values of the Yazd block suggest the presence of a possible sedimentary basin  
187 parallel to the Zagros trend. Despite the presence of igneous rock outcrops in the northern part of  
188 the Lut block, the low susceptibility anomaly suggests the presence of a sedimentary basin in this  
189 region, similar to the Tabas and Yazd blocks. Our results show an unexpected NNW-SSE  
190 extension of the Yazd-Tabas basins into central Iran with extremely low average crustal

191 susceptibility which is almost 250 km long in the NNW-SSE direction and around 150 km wide.  
192 **(Figure 1 and 8).**

193 The western Alborz low susceptibility anomaly suggest a large sediment volume or limited  
194 magmatic activity and/or ophiolite emplacement in comparison to the eastern Alborz. Further,  
195 high average susceptibility indicates that the Sabzevar magmatic ophiolite belt may extend SW-  
196 ward below the Great Kavir sedimentary basin (**Figure 1, 6 and 7**). The Great Kavir basin,  
197 despite the low relief, shows relatively high average susceptibility and sporadic anomalies.

198 The high susceptibility anomaly in the Jazmurian depression, in the SE corner of the SSZ,  
199 suggests the presence of igneous and/or oceanic crustal rocks beneath the sedimentary cover,  
200 whereas the low susceptibility anomaly in the NW of SSZ (NE front of Kermanshah ophiolites)  
201 suggests the presence of a local basin.

202 **Ophiolite belts:** In this study, we observe direct correlation between ophiolite outcrops and high  
203 average susceptibility anomalies in the Iranian plateau (**Figure 3 and 6**). In the Zagros suture  
204 zone, the high susceptibility anomalies of the Neyriz ophiolite continues to the NE below the  
205 sedimentary cover, suggesting that the ophiolite extends under the sedimentary cover. Lower  
206 intensity of the susceptibility anomaly suggests that the volume of the Kermanshah ophiolites is  
207 smaller than for the Neyriz ophiolites.

208 The Makran ophiolite is characterized by very high susceptibility with a sharp northward  
209 increase in amplitude at the edge of the ophiolite outcrops. The anomaly extends further north as  
210 a high-amplitude broad zone despite lack of outcrops at surface of ophiolite or igneous rocks.  
211 This observation suggests a northward extension of the Makran ophiolites and/or Cretaceous age  
212 igneous rocks beneath the sedimentary cover (**Figure 3 and 6**). The Cretaceous igneous rocks,

213 located in the south and north of Jazmurian depression (**Figure 3**), are emplaced during a age  
214 rifting event that was active during Jurassic-early Cretaceous (Burg, 2018). .

215 In Eastern Iran, the Sistan zone ophiolites have high susceptibility in two arch-shaped anomalies.  
216 We name the arch-shaped anomalies the Southern Sistan Magmatic Arc (SSMA) and the  
217 Northern Sistan Magmatic Arc (NSMA) magmatic anomalies (**Figure 11**). The SSMA matches  
218 with ophiolite outcrops in the south but bends toward the west into a zone where possible  
219 ophiolite are covered by sedimentary rocks, and the shape of the NSMA anomaly has the same  
220 trend as the SSMA.

221 Based on the susceptibility map we interpret the Sabzevar zone and Great Kavir Basin with their  
222 thick sedimentary cover as one tectonic block between Afghanistan and central Iran, which is  
223 southward limited by the Darounch strike-slip fault. In the western part of Sabzevar-Great Kavir  
224 zone the high susceptibility anomalies, mostly, coincide with ophiolites, while, toward to the  
225 west igneous rocks are dominant at the surface.

226 **Magmatic zones:** Geological mapping identifies four major magmatic areas in the Iranian  
227 Plateau (Figure 3): 1- The Tertiary Urumieh–Dokhtar Magmatic Arc (UDMA). 2- The Mesozoic  
228 Sanandaj-Sirjan magmatic arc. 3-Sabzevar – Kavir magmatic ophiolite belt and 4- Lut volcanic-  
229 plutonic belt of central eastern Iran (**Figure 3**).

230 Our results show a strong correlation between high average susceptibility and the location of  
231 surface outcrops of all these magmatic zones (**Figure 6**), in particular along the Urumieh–  
232 Dokhtar Magmatic Arc. This observation motivates us to identify new magmatic belts from the  
233 average susceptibility. Toward the SW of the Urmia-Dokhtar magmatic arc, the average  
234 susceptibility value in the Sanandaj-Sirjan zone is higher than in the Zagros Belt, which indicates

235 tectonic differences between Zagros and SSZ. Sporadic high susceptibility anomalies indicate a  
236 sporadic distribution of the Mesozoic age magmatic outcrops and ophiolites in the Sanandaj-  
237 Sirjan zone.

238 Our results show a remarkable correlation between igneous rock outcrops and high susceptibility  
239 anomalies in the magmatic-ophiolite belt of the Sabzevar-Great Kavir. The high susceptibility  
240 anomaly in the middle of Lut block does not match any outcrop of igneous rocks, probably, due  
241 to sediment cover, but suggest the presence of large magmatic/ophiolite bodies.

242 The Yazd block is separated from the Tabas block by a linear susceptibility anomaly, where the  
243 parts with sporadic high susceptibility correspond to outcrops of Precambrian age rocks (**Figure 3**  
244 **and 6**). These Precambrian outcrops represent an intense, approximately east-west striking Eocene  
245 crustal extension that formed a ~400-km-long NE-SW belt of metamorphic core complexes, which  
246 now are localized along the boundary between the Yazd and Tabas tectonic blocks (Verdel et al.,  
247 2007) as highlighted by the large average susceptibility values.

## 248 **5. Discussion:**

249 A first-order observation confirms that mapped mafic igneous and ophiolite rocks correspond  
250 to areas with strong positive average susceptibility, and that the major sedimentary basins  
251 correspond to areas with the lowest values of average susceptibility (Figure 5). The strong  
252 correlation between susceptibility anomalies and surface magmatic - ophiolite outcrops  
253 motivate us to extend our interpretation to other regions with anomalous susceptibility and  
254 less constrained tectonics. We have earlier demonstrated that variation in magnetic  
255 susceptibility, along a NE-SW striking profile in NW Iran, may identify sutures and terranes  
256 (Teknik et al., 2019). Furthermore, the susceptibility contrast between the crystalline

257 basement and sediment cover has been used for mapping magnetic basement in the Iranian  
258 plateau (Teknik and Ghods, 2017). Similar to our study, Munt et al. (2012) attributed the  
259 residual gravity anomaly to the upper crustal structures such as deep basins, igneous and  
260 ophiolite complexes. The basins with salt deposits are characterized by negative values  
261 ( $\sim -20$  mGal) and positive anomalies are related to the shallow basement depths and igneous-  
262 ophiolite rocks ( $\sim 20$  mGal). In addition to the sparsity of the terrestrial gravity data of Iran,  
263 the order of susceptibility contrast between igneous- ophiolite (generally; crystalline) rocks  
264 and sedimentary rocks are much higher than density contrast. Therefore, we find that the  
265 magnetic data can better show these contrasts. The residual gravity anomaly map by Munt et  
266 al. (2012) partially confirms correlation between distribution of igneous and ophiolite, but  
267 our results highlights the efficiency of our method.

### 268 *5.1 Sedimentary Basins*

269 The low average susceptibility anomaly in the best known basins of the study area (e.g.  
270 Zagros, Makran, Kopeh-Dagh, and Tabas) is caused by the presence of a thick, non-  
271 magnetized sedimentary cover. This implies that these basins have not been subject to mafic  
272 magmatic activity and ophiolite emplacement, at least in the upper sequences. We observe  
273 sporadic susceptibility anomalies in the eastern part of the Alborz and Jazmurian depression  
274 and Great Kavir sedimentary basin which indicates the presence of volcanic and magmatic  
275 rocks at depth in the sedimentary cover.

276 Despite hydrocarbon exploration in the major Zagros, Makran and Kopeh-Dagh basins,  
277 thickness and surface extent of basins in the Iranian plateau are still uncertain. The intra-  
278 plateau Tabas block has been subject to geological studies (e.g. Konon et al., 2016) which

279 show that it is fault bounded. No igneous intrusions have been mapped within the Tabas  
280 block, probably due to thick sedimentary cover. By analogy to the Zagros-Makran system,  
281 we interpret low, homogeneous susceptibility values by the presence of a large, deep  
282 sedimentary basin without magmatic rocks. We propose that the Tabas basin extends  
283 northwestward into the Yazd block (Figure 8) and that its northern and southern boundaries  
284 do not coincide with the suggested boundaries of the Tabas block (**Figure 8**) (Berberian and  
285 King, 1981; Talbot and Alavi, 1996). Large scale dextral transtension along the bounding  
286 faults may have created the Tabas basin as proposed by Konon et al., (2016), e.g. during  
287 counterclockwise rotation of the tectonic Lut, Tabas, and Yazd blocks (Şengör, 1990b).  
288 Another explanation may be related to westward subduction of ancient Sistan oceanic crust  
289 under the Lut block (Verdel et al., 2007).

290 The core complex zone between the Yazd and Tabas blocks (Verdel et al., 2007), includes  
291 Precambrian crystalline units that contrast the Mesozoic and younger rocks in the two blocks.  
292 The high susceptibility along this zone suggests that the sedimentary cover is thin, possibly  
293 due to early Miocene erosional exhumation (Şengör, 1990b; Verdel et al., 2007).

294 The Zagros suture is characterised by a sharp susceptibility contrast, which we attribute to  
295 compositional variation in the near surface rocks, noting that the susceptibility usually is  
296 higher in metamorphic than sedimentary rocks (**Figure 2**). The NW and SE parts of SSZ  
297 have relatively low average susceptibility with sporadic high susceptibility spots that indicate  
298 a dispersed distribution of ophiolites, e.g. at the Kermanshah and Neyriz ophiolites zones  
299 (**Figure 6 and Figure 7**). Our results suggest that these ophiolites connect under the  
300 sedimentary cover along the strike of the SSZ. Low susceptibility in the central part of the

301 SSZ, in agreement with surface geological observations, indicates the absence of magmatic  
302 and ophiolite complexes.

303 In the SE end of the SSZ, the high susceptibility anomaly suggests that the Makran ophiolites  
304 may extend beneath the sediment cover of the Jazmurian depression (**Figure 11**). The  
305 Juzmurian depression may be a remnant of a back-arc basin below the present-day Jazmurian  
306 basin (e.g. Burg 2018) or a fore-arc basin of the Urumieh-Dokhtar Magmatic arc (e.g. Alavi,  
307 1994; Alavi, 2007). Cretaceous magmatic rocks are located at the northern and southern  
308 border of the Jazmurian depression (Figure 3) around an extensional area (Burg 2018). We  
309 speculate that the northward extent of the Makran high susceptibility may indicate the  
310 presence of Cretaceous magmatic rocks beneath the Jazmurian sediments.

### 311 *5.2 Magmatic arcs and their relation to paleo-subduction properties*

312 Subduction zones are sites where tectonic processes destroy oceanic lithosphere and form  
313 new magmatic material that may be the building blocks of new continental crust (Tatsumi  
314 2005). Magmatic arcs usually exhibit some characteristics of their associated subduction  
315 system. Two global studies demonstrate that the volcanic arc width (Tatsumi and Eggins,  
316 1997) and the depth to the top of the zones of intermediate-depth seismicity beneath arc  
317 volcanoes (England et al., 2004) show negative linear correlation with the subduction angle.  
318 We use the results by Tatsumi and Eggins (1997) to estimate the paleo-dip of subduction  
319 systems related to the MOAs in Iran from the distance between the trench and magmatic arcs  
320 (Figure 9).

321 **Urmia Dokhtar Magmatic Arc (UDMA):** The magnetic susceptibility results indicate that  
322 the UDMA may be divided into the 600 km long and up/to 200 km wide Azarbayjan-Alborz

323 Magmatic Arc (AAMA) north of 34° N, and the 1300 km long and 50 to 60 km wide Arak-  
324 Jazmurian magmatic arc (AJMA) (Figure 8). The width of the magmatic arcs indicates very  
325 shallow subduction with a dip of <20 ° for AAMA, whereas the AJMA was characterized by  
326 steep subduction at an angle of 50 ° to 70 ° dip (Figure 9 and Figure 10). Shallow subduction  
327 requires a buoyant slab. The absence of magmatic activity in the Alborz to the east of the  
328 Damavand volcano suggests shallow subduction.

329 **The Central Iran magmatic activity:** Eastern Iran includes a series of volcanic–plutonic  
330 ophiolite complexes which extend ca. 1000 km southward from the Sabzevar-Kavir MOA  
331 into the Lut block. The Sabzevar-Kavir MOA includes arch-shaped anomalies typical of  
332 island arcs. Their width of 100 km in the east and 200 km in the west suggests that the  
333 subduction angle had an east to west decrease from 50° to less than 20° (Figure 9). Our data  
334 indicate that this igneous complex extends westward into the Great Kavir basin.

335 In Eastern Iran, despite the occurrence of massive magmatic and ophiolitic belts, there are no  
336 clear magnetic arc-shaped patterns reported in the geology maps and studies. We observe two  
337 clear parallel arc-shaped, high-susceptibility belts below the sedimentary cover in eastern  
338 Iran which have never been identified before (**Figure 11**). We propose that these anomalies  
339 represent two hitherto unknown magmatic arcs, which we name Southern Sistan Magmatic  
340 Arc (SSMA) and Northern Sistan Magmatic Arc (NSMA). We suggest that these two arcs are  
341 part of a Mesozoic magmatic arc at the Sistan suture zones, which are bended and segmented  
342 due to anti clockwise rotation of the Lut block (Mattei et al., 2012) in response to the  
343 convergence between the Arabian plate and the rigid Eurasian plate. Another interpretation  
344 may suggest that two independent magmatic arcs formed by lateral displacement of the



345 subduction system, possibly after accretion of a micro-continent which today is located  
346 between the two magmatic arcs.

347 The length of each arc is ca 400-450 km and the width is ca 40 km to 60 km similar to the  
348 AJMA, corresponding to a dip angle of ca. 60° (**Figure 9** and **11**). The existence of two  
349 parallel magmatic arcs is unusual and we are unaware of any tectonic analogues, although  
350 deformation of the Paleozoic subduction complexes in Asia created a series of repeated  
351 magmatic complexes similar to the Altai (Şengör et al., 2014). However, by slab retreat  
352 the same subduction system could have sourced the two parallel zones, which then would  
353 represent two paired zones of volcanoes as proposed by Tatsumi (2005). In this case, the joint  
354 system would be ca. 200 km wide, corresponding to a subduction dip angle of <20°.

355 **Regions with poor correlation of susceptibility and MOA:** Two areas with known  
356 presence of igneous and ophiolite rocks are characterized by low average susceptibility,  
357 mainly NW of the SSZ and north of the Lut block beneath Darouneh fault (**Figure 1,4 and**  
358 **6**). We speculate that the low susceptibility values may be caused by alteration of the original  
359 rocks or by effects from remnant magnetization in the opposite direction of the induced  
360 magnetization. An inherent assumption of the RAPS method is that remnant and induced  
361 magnetization must be parallel and in the same direction. This observation indicates  
362 uncertainty in our results here and a different origin and deformation history of these  
363 magmatic arcs from other arcs of the Iranian Plateau.

364 A discontinuous Mesozoic magmatic arc is indicated by scattered Jurassic to Cretaceous  
365 intrusive rocks from the Sanandaj Sirjan zone to Makran and further to the easternmost part  
366 of Lut (**Figure 3**) (Berberian and Berberian, 1981; Sengör 1990b). There is no significant

367 correlation with Mesozoic magmatic outcrops. It has been proposed that the high  
368 susceptibility value for Paleogene arcs in central and northern Iran, relative to the Mesozoic  
369 arc, reflects different source of magmatism as discussed by Verdel et al. (2011). This  
370 interpretation proposes that the two parallel easternmost anomalies may derived from  
371 ophiolites, in analogy to the Kermashah and Neyriz ophiolite in the SSZ (Figure 8).

## 372 **6. Conclusion**

373 We have applied the RASP method to calculate and map the average magnetic susceptibility in  
374 Iran. The results demonstrate that known occurrences of Magmatic-Ophiolite Arcs (MOA)  
375 correlate with high average susceptibility areas, although the calculated susceptibility is low at  
376 two MOAs. We conclude that magnetic susceptibility is a useful parameter for identification of  
377 MOAs in areas with sparse geological information, be it due to a remote location or thick  
378 sedimentary cover.

379 We discover two parallel, hitherto unknown MOAs in eastern Iran which developed in a steeply  
380 dipping ( $>60^\circ$  dip) subduction zone, although we cannot completely rule out that they represent  
381 paired lines of volcanoes in a system with shallow subduction. Our results indicate shallow  
382 subduction ( $<20^\circ$  dip) of the Neo-Tethys ocean in the NW (AMAA) and SE parts of the Alborz  
383 as well as in the Sabzevar-Kavir MOA. In contrast, the major, central part (AJMA) of the Alborz  
384 and the newly discovered eastern MOAs formed in steeply dipping ( $>60^\circ$  dip) subduction  
385 systems. Based on the magnetic susceptibility results we identify new boundaries of the  
386 economically valuable Tabas sedimentary basin.

## 387 **Acknowledgment**

388 This work was carried out at Istanbul Technical University-Eurasia Institute of Earth Science and  
389 the IASBS. VT is financed by a grant from the ITU BAP programme (Project #42338 titled

390 “Potential field modeling of structures related to the amalgamation of Anatolia”) and grants from  
391 DFF-1323-00053, FNU16-059776-15 from the Danish Research Council and sabbatical grant  
392 from IASBS.

393

394 **6.** (Maus and Dimri, 1995b)

395 **7. References**

396 Alaminia, Z., Karimpour, M.H., Homam, S.M., Finger, F., 2013. The magmatic record in the  
397 Arghash region (northeast Iran) and tectonic implications. *Int. J. Earth Sci.* 102, 1603–1625.  
398 <https://doi.org/10.1007/s00531-013-0897-1>

399 Arjmandzadeh, R., Karimpour, M.H., Mazaheri, S.A., Santos, J.F., Medina, J.M., Homam, S.M.,  
400 2011. Sr-Nd isotope geochemistry and petrogenesis of the Chah-Shaljami granitoids (Lut  
401 Block, Eastern Iran). *J. Asian Earth Sci.* 41, 283–296.  
402 <https://doi.org/10.1016/j.jseaes.2011.02.014>

403 Ballato, P., Uba, C.E., Landgraf, A., Strecker, M.R., Sudo, M., Stockli, D.F., Friedrich, A.,  
404 Tabatabaei, S.H., 2011. Arabia-Eurasia continental collision: Insights from late Tertiary  
405 foreland-basin evolution in the Alborz Mountains, northern Iran. *Geol. Soc. Am. Bull.* 123,  
406 106–131. <https://doi.org/10.1130/B30091.1>

407 Berberian, F., Berberian, M., 1981. Tectono-plutonic episodes in Iran. pp. 5–32.  
408 <https://doi.org/10.1029/GD003p0005>

409 Berberian, M., 1995. Master “blind” thrust faults hidden under the Zagros folds: active basement  
410 tectonics and surface morphotectonics. *Tectonophysics.* [https://doi.org/10.1016/0040-](https://doi.org/10.1016/0040-1951(94)00185-C)  
411 [1951\(94\)00185-C](https://doi.org/10.1016/0040-1951(94)00185-C)

412 Berberian, M., 1983. The southern Caspian: A compressional depression floored by a trapped,  
413 modified oceanic crust". *Can. J. Earth Sci.* 20, 163–183. <https://doi.org/10.1139/e83-015>

414 Berberian, M., King, G.C.P., 1981. Towards a paleogeography and tectonics evolution of Iran.  
415 *Can. J. Earth Sci.* <https://doi.org/10.1017/CBO9781107415324.004>

416 Bouligand, C., Glen, J.M.G., Blakely, R.J., 2009. Mapping Curie temperature depth in the  
417 western United States with a fractal model for crustal magnetization. *J. Geophys. Res. Solid*  
418 *Earth* 114, 1–25. <https://doi.org/10.1029/2009JB006494>

419 Boulin, J., 1991. Structures in Southwest Asia and evolution of the eastern Tethys.  
420 *Tectonophysics* 196, 211–268. [https://doi.org/10.1016/0040-1951\(91\)90325-M](https://doi.org/10.1016/0040-1951(91)90325-M)

421 Burg, J.P., 2018. Geology of the onshore Makran accretionary wedge: Synthesis and tectonic  
422 interpretation. *Earth-Science Rev.* 185, 1210–1231.  
423 <https://doi.org/10.1016/j.earscirev.2018.09.011>

424 Clark, D.A., Emerson, D.W., 1991. Notes on rock magnetization characteristics in applied  
425 geophysical studies. *Explor. Geophys.* 22, 547–555. <https://doi.org/10.1071/EG991547>

426 Dewey, J., Pitman, W.C., Ryan, W.B.F., Bonnin, J., 1973. Plate Tectonics and the Evolution of  
427 the Alpine System. *Geol. Soc. Am. Bull.* 84, 3137. [https://doi.org/10.1130/0016-7606\(1973\)84<3137:PTATEO>2.0.CO;2](https://doi.org/10.1130/0016-7606(1973)84<3137:PTATEO>2.0.CO;2)

428

429 England, P., Engdahl, R., Thatcher, W., 2004. Systematic variation in the depths of slabs beneath  
430 arc volcanoes 377–408. <https://doi.org/10.1111/j.1365-246X.2003.02132.x>

431 Glennie, K.W., Hughes Clarke, M.W., Boeuf, M.G.A., Pilaar, W.F.H., Reinhardt, B.M., 1990.  
432 Inter-relationship of Makran-Oman Mountains belts of convergence. *Geol. Soc. London,*

433 Spec. Publ. <https://doi.org/10.1144/GSL.SP.1992.049.01.47>

434 Hunt, C.P., Moskowitz, B.M., Banerjee, S.K., 1995. Rock Physics & Phase Relations: A  
435 Handbook of Physical Constants. AGU Ref. Shelf 3, 189–204.  
436 <https://doi.org/10.1029/RF003>

437 Jackson, J., Priestley, K., Allen, M., Berberian, M., 2002. Active tectonics of the South Caspian  
438 Basin. *Geophys. J. Int.* 148, 214–245. <https://doi.org/10.1046/j.1365-246X.2002.01588.x>

439 Konon, A., Nadimi, A., Koprianiuk, M., Wysocka, A., Szaniawski, R., Wygl, M., 2016.  
440 Formation of intracontinental basins in the opposite corners of the Tabas block as coeval  
441 structures controlled by t .... Formation of intracontinental basins in the opposite corners of  
442 the Tabas block as coeval structures controlled by transpressional fa.  
443 <https://doi.org/10.1130/B31362.1>

444 Li, Y., Oldenburg, D.W., 1993. 3-D inversion of magnetic data. 1993 SEG Annu. Meet. 61, 400–  
445 402. <https://doi.org/10.1190/1.1822498>

446 Mattei, M., Cifelli, F., Muttoni, G., Zanchi, A., Berra, F., Mossavvari, F., Eshraghi, S.A., 2012.  
447 Neogene block rotation in central Iran : Evidence from paleomagnetic data 943–956.  
448 <https://doi.org/10.1130/B30479.1>

449 Maus, S., Dimri, V., 1995a. Potential field power spectrum inversion for scaling geology. *J.*  
450 *Geophys. Res.* <https://doi.org/10.1029/95JB00758>

451 Maus, S., Dimri, V., 1995b. Potential field power spectrum inversion for scaling geology. *J.*  
452 *Geophys. Res. Solid Earth* 100, 12605–12616. <https://doi.org/10.1029/95jb00758>

453 Maus, S., Gordon, D., Fairhead, D., 1997. Curie-temperature depth estimation using a self-

454 similar magnetization model. *Geophys. J. Int.* 129, 163–168. <https://doi.org/10.1111/j.1365->  
455 [246x.1997.tb00945.x](https://doi.org/10.1111/j.1365-246x.1997.tb00945.x)

456 McCall, G.J.H., Kidd, R.G.W., 1982. The Makran, Southeastern Iran: the anatomy of a  
457 convergent plate margin active from Cretaceous to Present. *Geol. Soc. London, Spec. Publ.*  
458 <https://doi.org/10.1144/GSL.SP.1982.010.01.26>

459 Nowroozi, A.A., 1971. Seismo-tectonics of the Persian plateau, eastern Turkey, Caucasus, and  
460 Hindu-Kush regions. *Bull. Seismol. Soc. Am.*

461 Richards, J.P., 2015. Tectonic, magmatic, and metallogenic evolution of the Tethyan orogen:  
462 From subduction to collision. *Ore Geol. Rev.* 70, 323–345.  
463 <https://doi.org/10.1016/j.oregeorev.2014.11.009>

464 Saleh, R., 2006. Reprocessing of aeromagnetic map of Iran. Institute for Advanced Studies in  
465 Basic Sciences.

466 Şengör, A.M.C., 1990. Plate tectonics and orogenic research after 25 years: A Tethyan  
467 perspective. *Earth-Science Rev.* 27, 1–201. [https://doi.org/10.1016/0012-8252\(90\)90002-D](https://doi.org/10.1016/0012-8252(90)90002-D)

468 Sepehr, M., Cosgrove, J., 2004. Structural framework of the Zagros Fold–Thrust Belt, Iran. *Mar.*  
469 *Pet. Geol.* 21, 829–843. <https://doi.org/10.1016/j.marpetgeo.2003.07.006>

470 Stampfli, G.M., Borel, G.D., 2002. A plate tectonic model for the Paleozoic and Mesozoic  
471 constrained by dynamic plate boundaries and restored synthetic oceanic isochrons. *Earth*  
472 *Planet. Sci. Lett.* 196, 17–33. [https://doi.org/10.1016/S0012-821X\(01\)00588-X](https://doi.org/10.1016/S0012-821X(01)00588-X)

473 Stocklin, J., 1968. Structural History and Tectonics of Iran: A Review. *Am. Assoc. Pet. Geol.*  
474 *Bull.* 52, 1229–1258.

- 475 Teknik, V., Ghods, A., 2017. Depth of magnetic basement in Iran based on fractal spectral  
476 analysis of aeromagnetic data. *Geophys. J. Int.* 209, 1878–1891.  
477 <https://doi.org/10.1093/gji/ggx132>
- 478 Teknik, V., Ghods, A., Thybo, H., Artemieva, I.M., 2019. Crustal density structure of the  
479 northwestern Iranian Plateau. *Can. J. Earth Sci.* 56, 1347–1365. [https://doi.org/10.1139/cjes-](https://doi.org/10.1139/cjes-2018-0232)  
480 2018-0232
- 481 Verdel, C., Wernicke, B.P., Hassanzadeh, J., Guest, B., 2011. A Paleogene extensional arc flare -  
482 up in Iran. *Tectonics* 30, 1–20. <https://doi.org/10.1029/2010TC002809>
- 483 Verdel, C., Wernicke, B.P., Renne, P.R., Spell, T.L., 2007. Geology and thermochronology of  
484 Tertiary Cordilleran-style metamorphic core complexes in the Saghand region of central  
485 Iran 961–977. <https://doi.org/10.1130/B26102.1>
- 486
- Alaminia, Z., Karimpour, M.H., Homam, S.M., Finger, F., 2013. The magmatic record in the  
Arghash region (northeast Iran) and tectonic implications. *Int. J. Earth Sci.* 102, 1603–1625.
- Alavi, M., 1994. Tectonics of the Zagros orogenic belt of Iran: new data and interpretations.  
*Tectonophysics* 229, 211–238.
- Alavi, M., 2007. Structure of the Zagros fold-thrust belt in Iran. *Am. J. Sci.* 307 (9), 1064–1095.
- Amante, C., Eakins, B.W., 2009. ETOPO1 1 Arc-Minute Global Relief Model: Procedures, Data  
Sources and Analysis, NOAA Technical Memorandum NESDIS NGDC-24.
- Arjmandzadeh, R., Karimpour, M.H., Mazaheri, S.A., Santos, J.F., Medina, J.M., Homam, S.M.,  
2011. Sr-Nd isotope geochemistry and petrogenesis of the Chah-Shaljami granitoids (Lut  
Block, Eastern Iran). *J. Asian Earth Sci.* 41, 283–296.
- Ballato, P., Uba, C.E., Landgraf, A., Strecker, M.R., Sudo, M., Stockli, D.F., Friedrich, A.,  
Tabatabaei, S.H., 2011. Arabia-Eurasia continental collision: Insights from late Tertiary  
foreland-basin evolution in the Alborz Mountains, northern Iran. *Geol. Soc. Am. Bull.* 123,  
106–131.

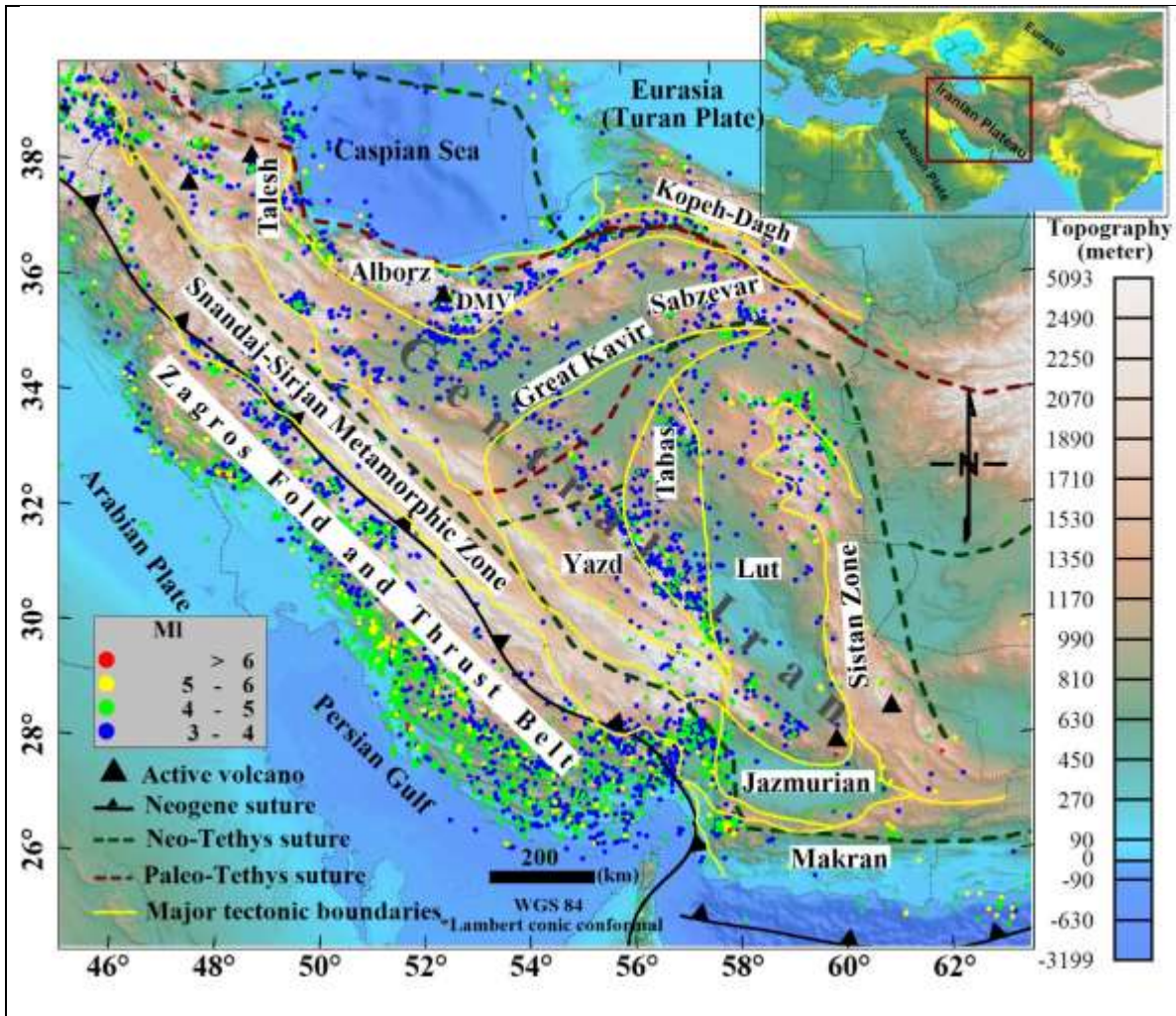
- Berberian, F., Berberian, M., 1981. Tectono-plutonic episodes in Iran. pp. 5–32.
- Berberian, M., 1983. The southern Caspian: A compressional depression floored by a trapped, modified oceanic crust". *Can. J. Earth Sci.* 20, 163–183.
- Berberian, M., 1995. Master “blind” thrust faults hidden under the Zagros folds: active basement tectonics and surface morphotectonics. *Tectonophysics*.
- Berberian, M., King, G.C.P., 1981. Towards a paleogeography and tectonic evolution of Iran. *Can. J. Earth Sci.* 18, 210–265.
- Bouligand, C., Glen, J.M.G., Blakely, R.J., 2009. Mapping Curie temperature depth in the western United States with a fractal model for crustal magnetization. *J. Geophys. Res. Solid Earth* 114, 1–25.
- Boulin, J., 1991. Structures in Southwest Asia and evolution of the eastern Tethys. *Tectonophysics*.
- Burg J. P., 2018. Geology of the onshore Makran accretionary wedge: Synthesis and tectonic interpretation. *Earth-Science Reviews*. 185, 1210-1231.
- Chiu, H.-Y., Chung, S.-L., Zarrinkoub, M. H., Mohammadi, S. S., Khatib, M. M., and Iizuka, Y., 2013, Zircon U–Pb age constraints from Iran on the magmatic evolution related to Neotethyan subduction and Zagros orogeny: *Lithos*, v. 162–163, p. 70–87, <https://doi.org/10.1016/j.lithos.2013.01.006>.
- Clark, D.A., Emerson, D.W., 1991. Notes on rock magnetization characteristics in applied geophysical studies. *Explor. Geophys.* 22, 547–555.
- Dewey, J.F., Pitman, W.C., Ryan, W.B.F., Bonnin, J., 1973. Plate Tectonics and the Evolution of the Alpine System. *Geol. Soc. Am. Bull.* 84, 3137.
- Engdahl, E.R., Jackson, J.A., Myers, S.C., Bergman, E.A., Priestley, K., 2006. Relocation and assessment of seismicity in the Iran region. *Geophys. J. Int.* 167, 761–778.
- Glennie, K.W., Hughes Clarke, M.W., Boeuf, M.G.A., Pilaar, W.F.H., Reinhardt, B.M., 1990. Inter-relationship of Makran-Oman Mountains belts of convergence. *Geol. Soc. London, Spec. Publ.*
- Hessami, K., Jamali, Tabassi, 2003. Major Active Faults of Iran. *Remote Sens. Environ.*
- Hunt, C.P., Moskowitz, B.M., Banerjee, S.K., 1995. *Rock Physics & Phase Relations: A Handbook of Physical Constants*. AGU Ref. Shelf 3, 189–204.
- Jackson, J., Priestley, K., Allen, M., Berberian, M., 2002. Active tectonics of the South Caspian Basin. *Geophys. J. Int.* 148, 214–245.
- McCall, G.J.H., Kidd, R.G.W., 1982. The Makran, Southeastern Iran: the anatomy of a convergent plate margin active from Cretaceous to Present. *Geol. Soc. London, Spec. Publ.*



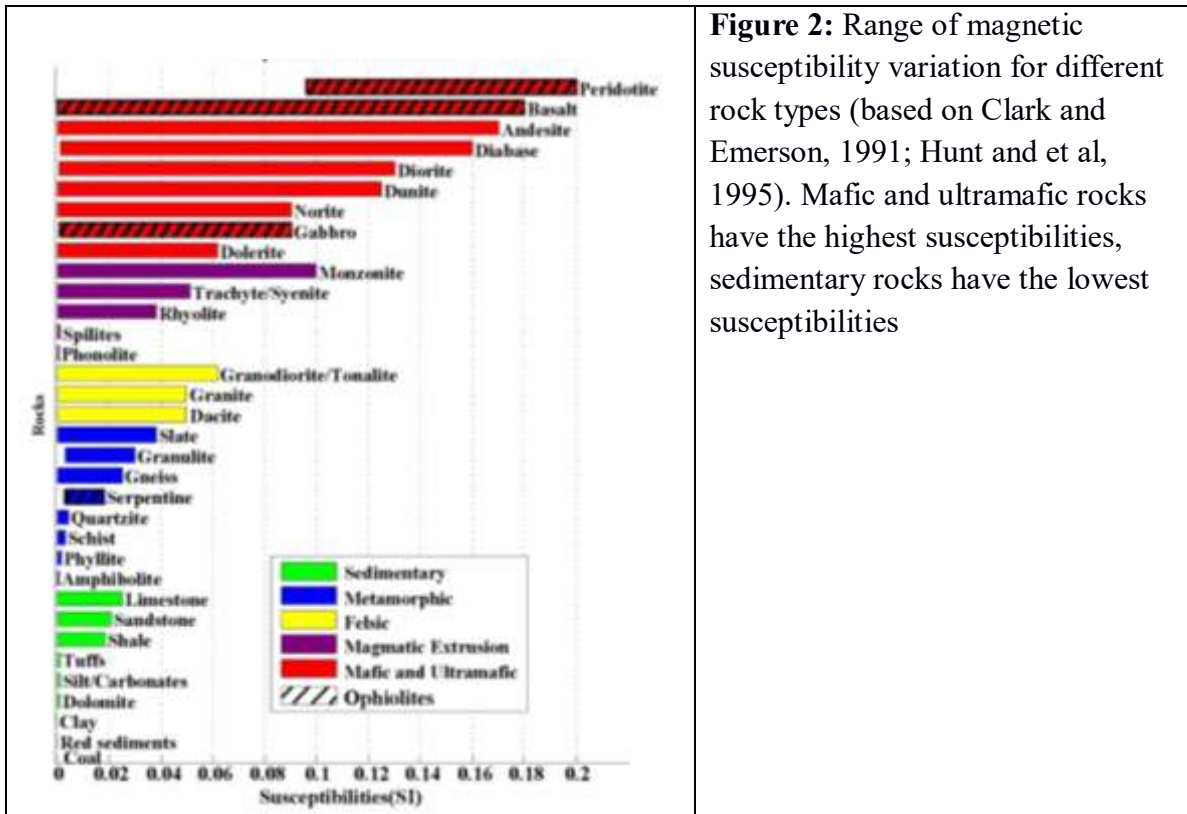
- Mattei, M., Cifelli, F., Muttoni, G., Zanchi, A., Berra, F., Mossavvari, F., Eshraghi, S.A., 2012. Neogene block rotation in central Iran: Evidence from paleomagnetic data 943–956. <https://doi.org/10.1130/B30479.1>
- Jiménez-Munt, M. Fernández, E. Saura, J. Vergés, D. Garcia-Castellanos, 3-D lithospheric structure and regional/residual Bouguer anomalies in the Arabia—Eurasia collision (Iran), *Geophysical Journal International*, Volume 190, Issue 3, September 2012, Pages 1311–1324, <https://doi.org/10.1111/j.1365-246X.2012.05580.x>
- Nogole-Sadat, M.A.A. and Almasian, M., 1993. Tectonic Map of Iran in 1:1000,000 Scale. Tehran.
- Nowroozi, A.A., 1971. Seismo-tectonics of the Persian plateau, eastern Turkey, Caucasus, and Hindu-Kush regions. *Bull. Seismol. Soc. Am.*
- Richards, J.P., 2015. Tectonic, magmatic, and metallogenic evolution of the Tethyan orogen: From subduction to collision. *Ore Geol. Rev.* 70, 323–345.
- Richards, J.P., Şengör, A.M.C., 2017. Did Paleo-Tethyan anoxia kill arc magma fertility for porphyry copper formation? *Geology* 45, 591–594.
- Saleh, R., 2006. Reprocessing of aeromagnetic map of Iran. Institute for Advanced Studies in Basic Sciences.
- Şengör, A.M.C., Natal'in, B.A., Sunal, G., van der Voo, R., 2014. A new look at the Altaids: A superorogenic complex in northern and central Asia as a factory of continental crust. Part I: Geological data compilation (Exclusive of palaeomagnetic observations). *Austrian J. Earth Sci.* 107, 169–232.
- Şengör A.M.C., 1990a. Plate tectonics and orogenic research after 25 years: A Tethyan perspective. *Earth-Science Rev.* 27, 1–201.
- Şengör A.M.C., 1990b. A new model for the late Palaeozoic-Mesozoic tectonic evolution of Iran and implications for Oman. In: Robertson AHF, Searle MP, Ries AC, editors. *The Geology and Tectonics of the Oman Region*. London, UK: Geological Society of London Special Publications, 797–831.
- Sepehr, M., Cosgrove, J.W., 2004. Structural framework of the Zagros Fold-Thrust Belt, Iran. *Mar. Pet. Geol.*
- Stampfli, G.M., Borel, G.D., 2002. A plate tectonic model for the Paleozoic and Mesozoic constrained by dynamic plate boundaries and restored synthetic oceanic isochrons. *Earth Planet. Sci. Lett.* 196, 17–33.
- Stern, R. J. 2002. Subduction zones. *Reviews of Geophysics*, 40(4), 1012. <https://doi.org/10.1029/2001RG000108>

- Stocklin, J., 1968. Structural History and Tectonics of Iran: A Review. *Am. Assoc. Pet. Geol. Bull.* 52, 1229–1258.
- Talbot, C.J., Alavi, M., 1996. The past of a future syntaxis across the Zagros. *Geol. Soc. London, Spec. Publ.* 100, 89–109.
- Tatsumi, Y., 2005. The subduction factory: How it operates in the evolving Earth. *GSA Today* 15, 4–10.
- Tatsumi, Y., Eggins, S., 1997. Subduction Zone Magmatism. *Surv. Geophys.*
- Teknik, V., Ghods, A., Thybo, H., Artemieva, I., 2019. Crustal density structure of NW Iranian Plateau. *Canadian J. of Earth Sciences*. DOI: 10.1139/cjes-2018-0232.
- Teknik, V., Ghods, A., 2017. Depth of magnetic basement in Iran based on fractal spectral analysis of aeromagnetic data. *Geophys. J. Int.* 209, 1878–1891.
- Verdel, C., Wernicke, B. P., Hassanzadeh, J., Guest, B., 2011. A Paleogene extensional arc flare up in Iran. *Tectonics*, 30, TC3008, doi:10.1029/2010TC002809.
- Verdel, C., Wernicke, B.P., Renne, P.R., Spell, T.L., 2007. Geology and thermochronology of Tertiary Cordilleran-style metamorphic core complexes in the Saghand region of central Iran 961–977. doi:10.1130/B26102.1

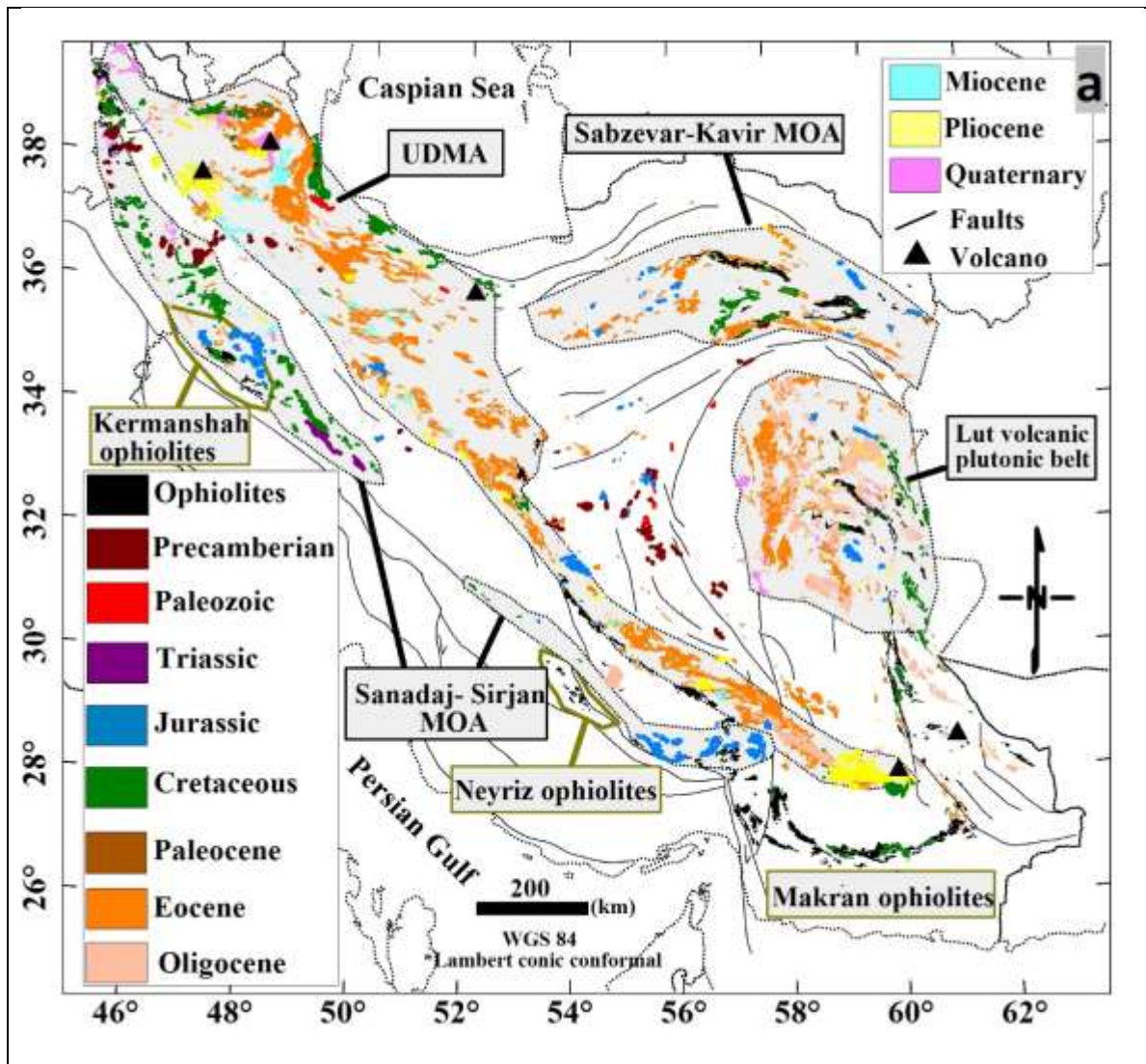
## Figures



**Figure 1:** Topography of the Iranian plateau based on the ETOPO 1 global elevation model (Amante and Eakins, 2009) with main tectonic structures superimposed. Thick lines represent major suture zones associated with the Paleo-Tethys (Permian to Jurassic) and Neo-Tethys oceans (Cretaceous–Cenozoic) subduction and collision closures (after Richards and Şengör, 2017) and yellow bold lines outline other main tectonic features (after Nogole-Sadat and Almasian, 1993). Colored dots mark earthquake epicenters and magnitudes (MI in the figure) from Engdahl et al. (2006) for the period of 1964-1998, supplemented by recently collected data by Institute of Geophysics of Tehran University (IGUT) from the Iranian Seismological Center website ([irsc.ut.ac.ir/bulletin.php](http://irsc.ut.ac.ir/bulletin.php) last download March 2017). The IRSC catalogue is searched for magnitude larger than 3.0 and azimuthal gap smaller than 120. The tectonically active part of the Iranian Plateau is defined by broad bands of seismicity concentrated in belts around small, relatively stable blocks.







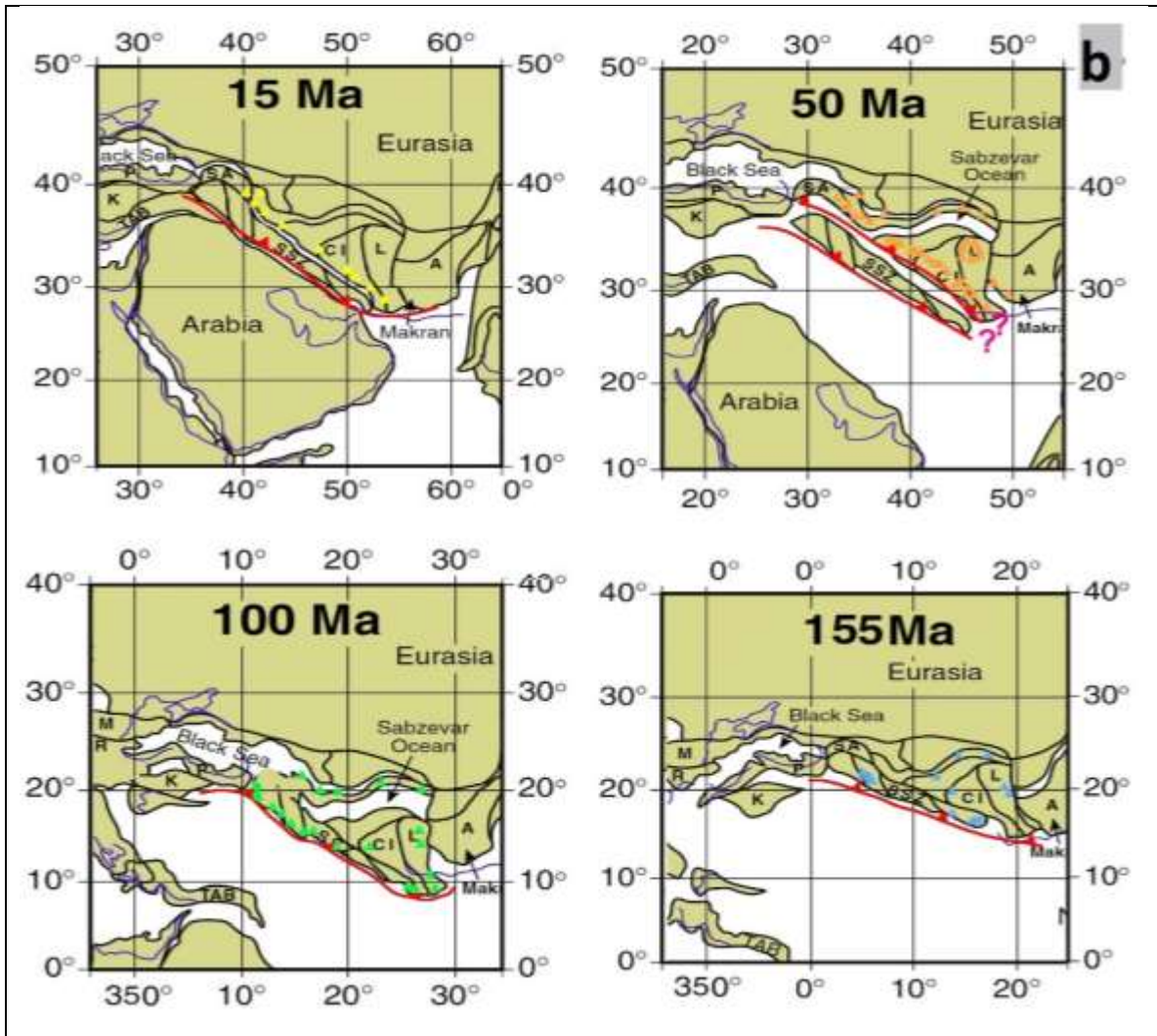


**Figure 3: a)** Location and age of mapped magmatic rocks and four major magmatic zones in Iran based on 1:100 000 scale maps from the Geological Survey of Iran.

**b)** Paleogeographic reconstructions of the central Neo-Tethys realm (after Richards 2015). Blue lines represent present-day coastlines, for reference. The red line indicates the subduction places. The triangles indicate the distribution of magmatism inferred from magmatic map (**Figure 3a**) and colours of the triangles indicate age according to the magmatic map (**Figure 3a**).

Abbreviations: UDMA – Urumieh-Dokhtar Magmatic Arc; MOA – Magmatic Ophiolite Arc; A – Afghan block; CI – Central Iranian block; K – Kırşehir block; L – Lut block; P – Pontides; SA – South Armenian block; SSZ – Sanandaj Sirjan Zone; TAB – Tauride Anatolide block.

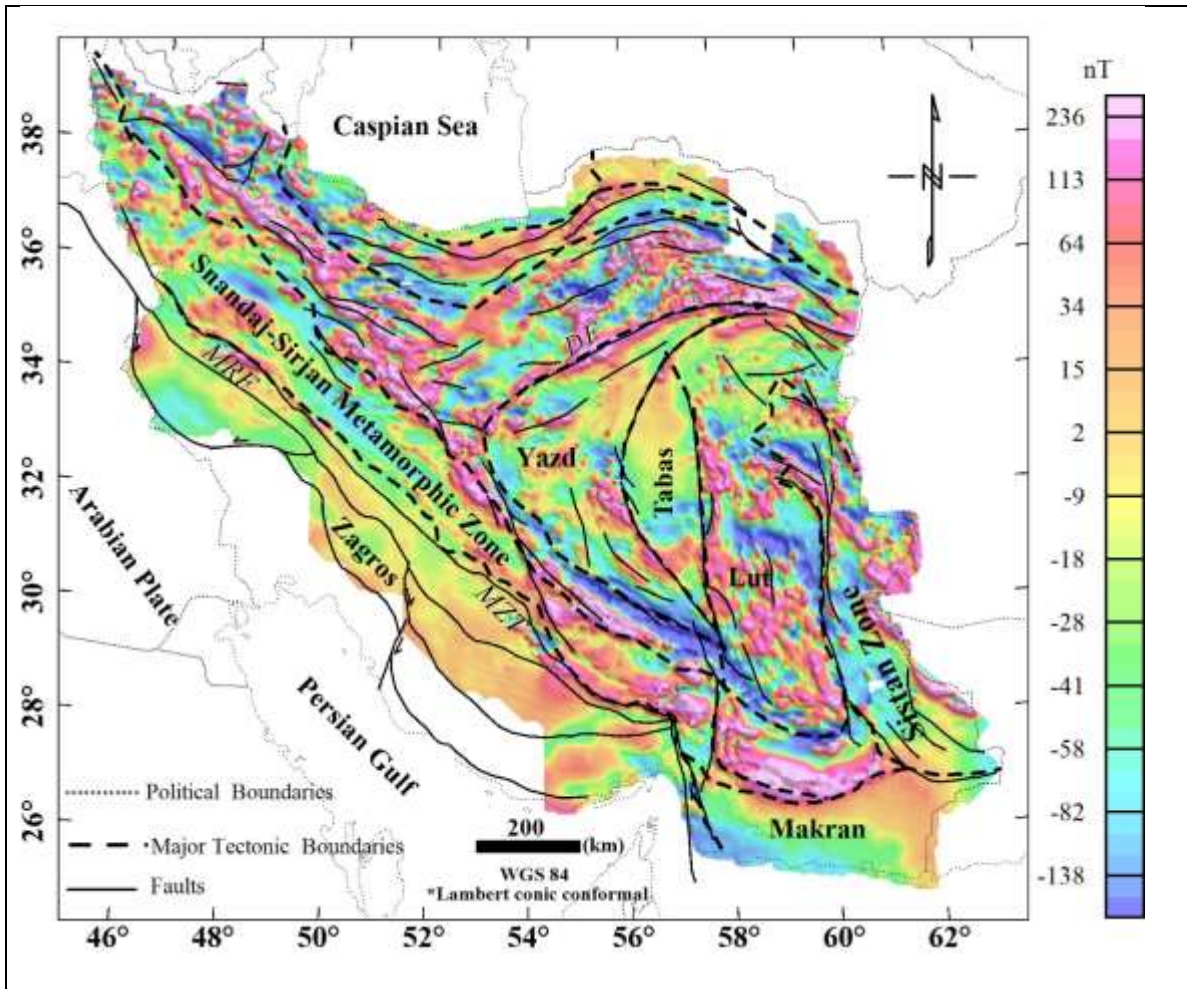


**Figure 4:** Aeromagnetic map of Iran (after Saleh, 2006). The black solid lines show the surface traces of active faults (after Hessami et al., 2003). Abbreviations: DF-Darouneh Fault; MZT - Main Zagros Thrust; MRF-Main Recent Fault.



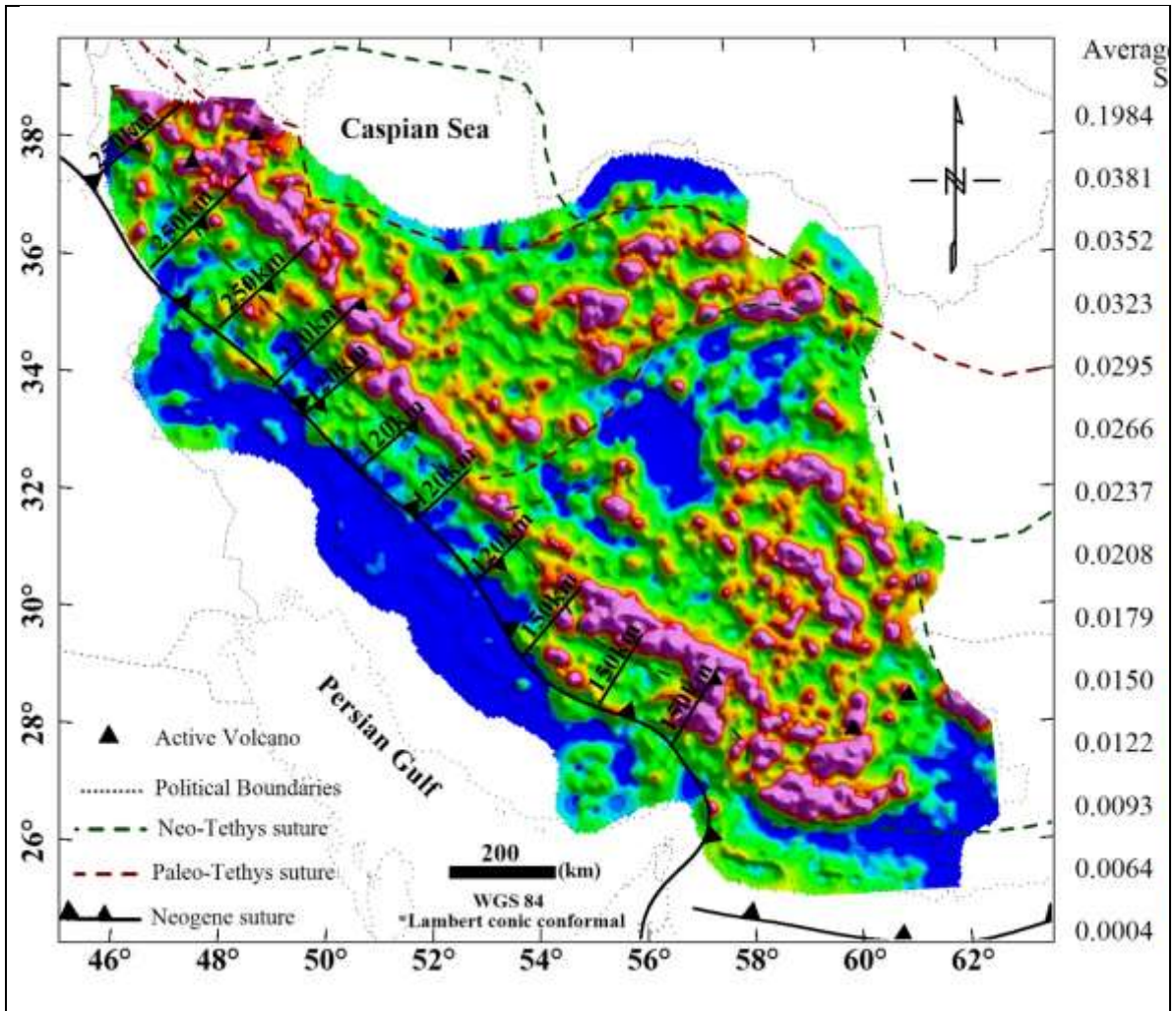


**Figure 5:** Calculated average crustal susceptibility of Iran overlain by (thick dashed lines) suture zones (after Richards and Şengör, 2017). Resolution is limited by the  $80 \times 80$  km horizontal averaging and the vertical averaging from the surface to the Curie Depth Point (CDP). Present-day arc-trench distances along Urmia Dokhtar Magmatic Arc are marked at selected locations.



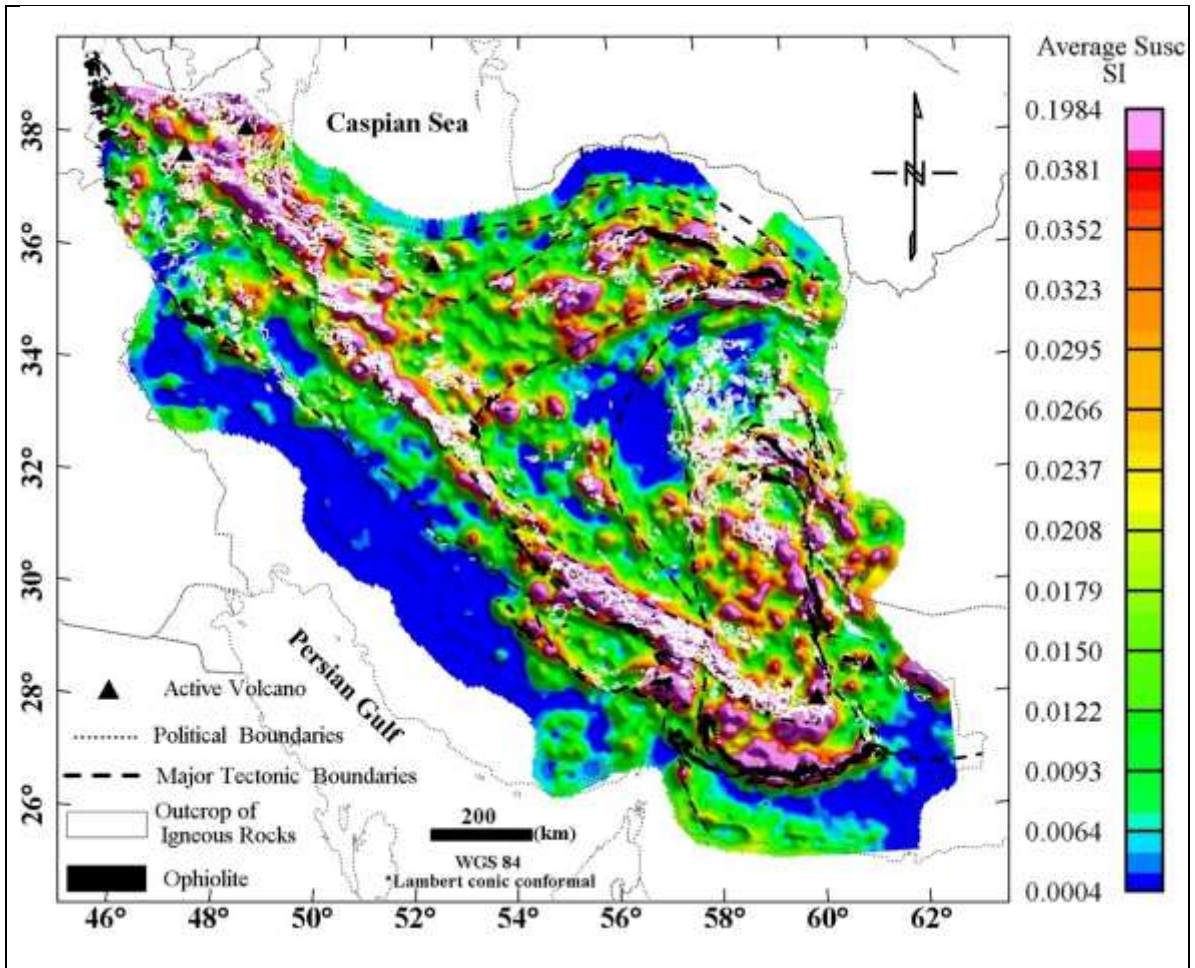


**Figure 6:** Average susceptibility map overlain by locations of surface outcrops of igneous rocks and ophiolites (thin white and black lines, respectively). Black dashed lines are borders of geological units (after Nogole-Sadat and Almasian, 1993).

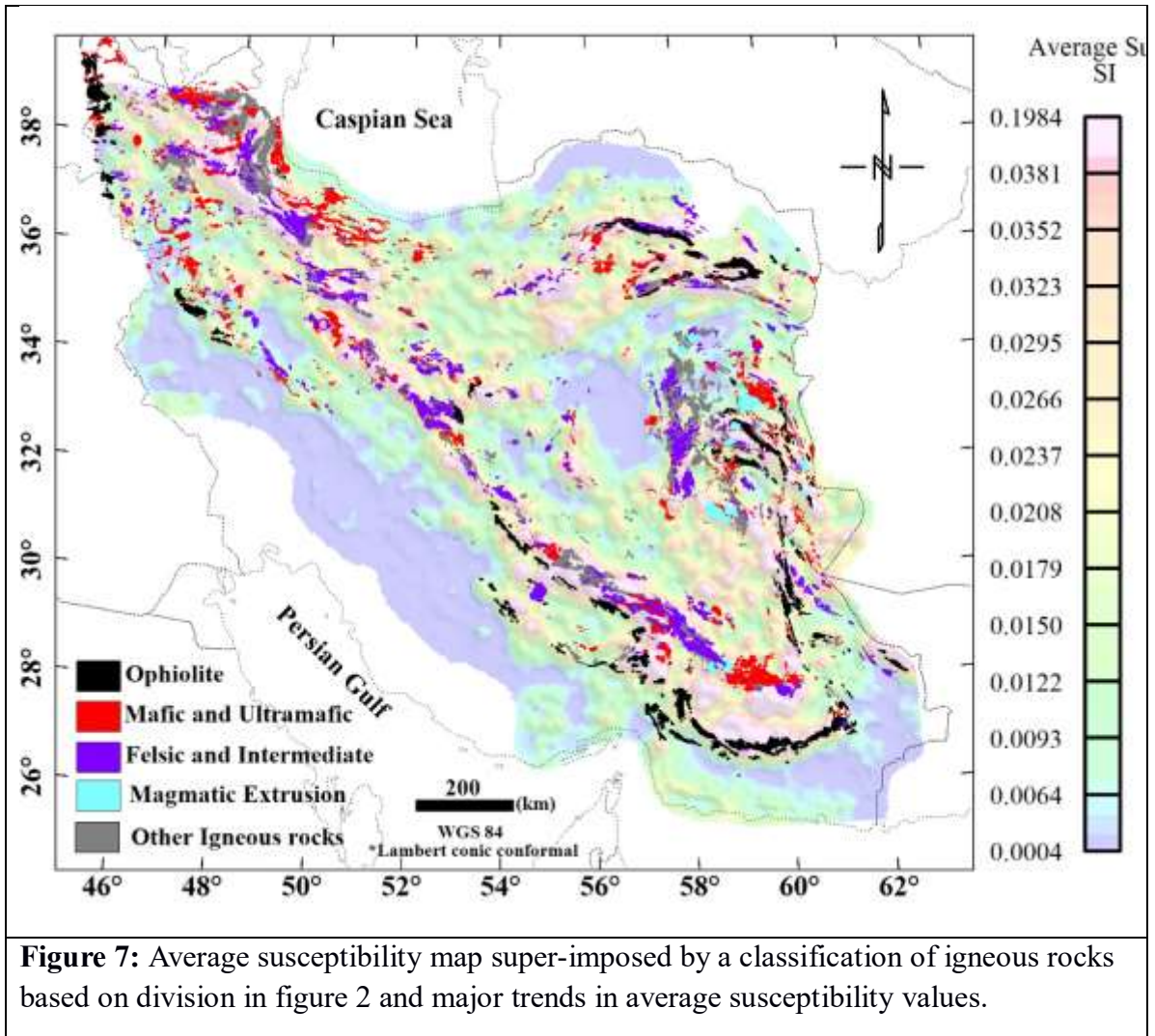


**Figure 7:** Average susceptibility map super-imposed by a classification of igneous rocks based on division in figure 2 and major trends in average susceptibility values.

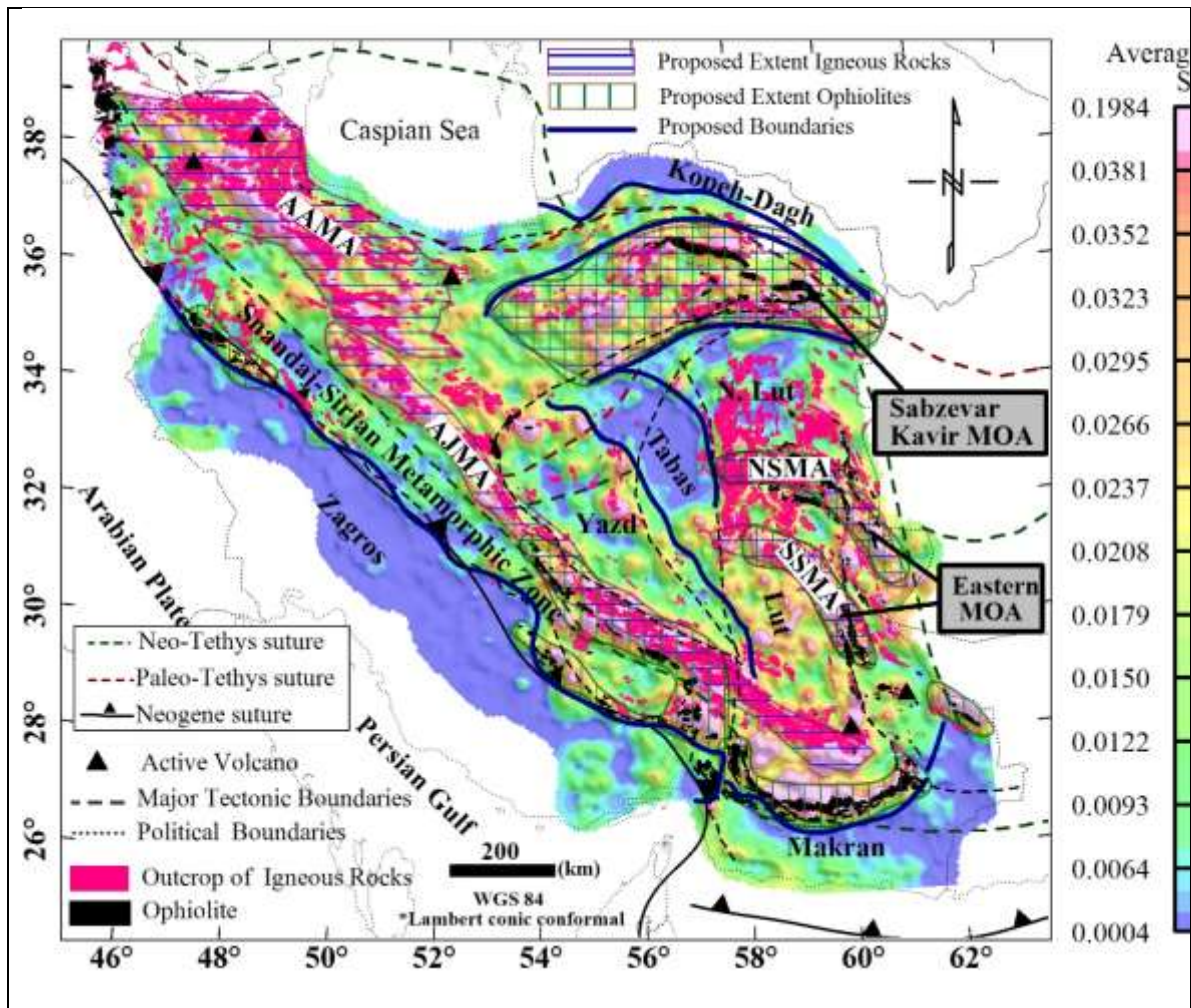


**figure 8:** New tectonic interpretation based on average susceptibility and correlation with distribution of outcropped ophiolite and igneous rocks. Results shows that the Urmia Dokhtar Magmatic Arc (UDMA) can be divided into a wide and curved Azarbayjan-Alborz Magmatic Arc (AAMA) in the NW and a narrow and straight Arak-Jazmurian Magmatic Arc (AJMA) from central Iran to SE of Iran. We recognize the Tabas basin as a tectonic province with new properties and we revise the boundaries between Tabas and Yazd blocks. We also interpreted two new parallel arch shapes in eastern Iran including Southern Sistan Magmatic Arc (SSMA) and Northern Sistan Magmatic Arc (NSMA)

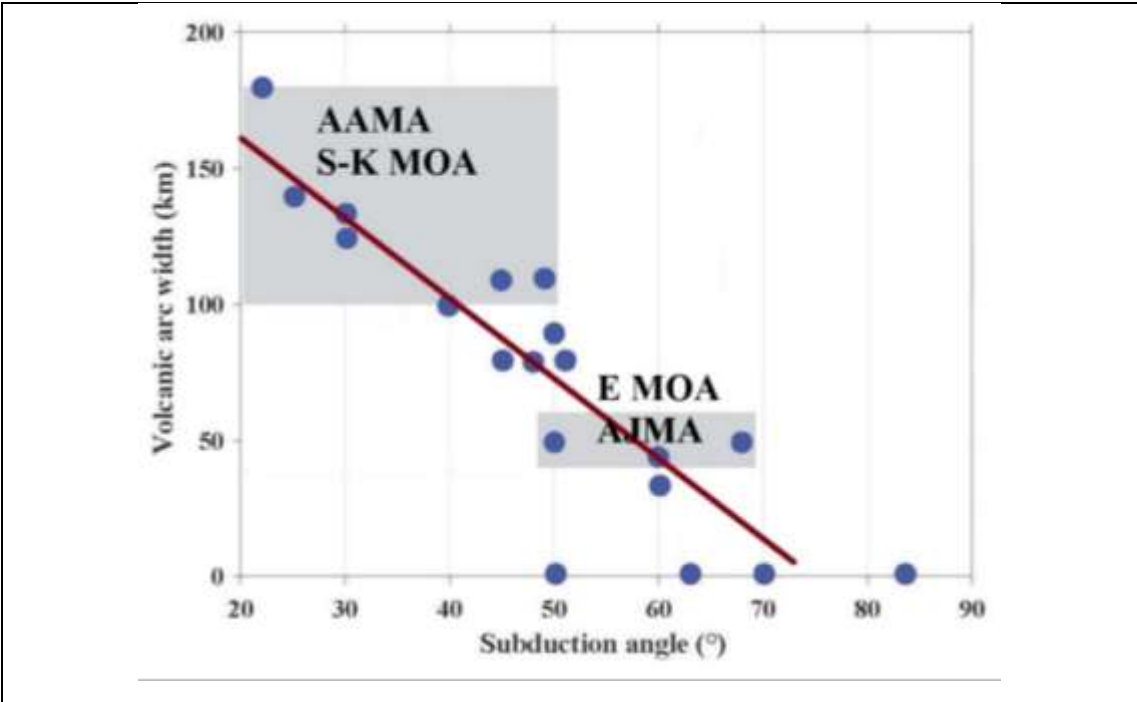


**Figure 9:** Tectonic characteristics of subduction zone magmatism demonstrating a negative correlation between subduction angle and volcanic arc width (blue circles; Tatsumi and Eggin, 1997). The width of the grey rectangles corresponds to the range of width of the inferred magmatic belts (100-180 km for AAMA and S-K MOA; and 40-60 km for E MOA and AJMA), and the length of the rectangles indicate the range of estimated subduction angle. The red line indicates the best fit line and the crossing points with grey rectangles indicate the mean value volcanic arc width and subduction angle for each arc. Abbreviations: AAMA: Azarbayjan-Alborz Magmatic Arc; S-K MOA: Sabzevar-Kavir magmatic-ophiolite arc; E MOA: Eastern magmatic-ophiolite arc; and AJMA: Arak-Jazmurian magmatic arc.



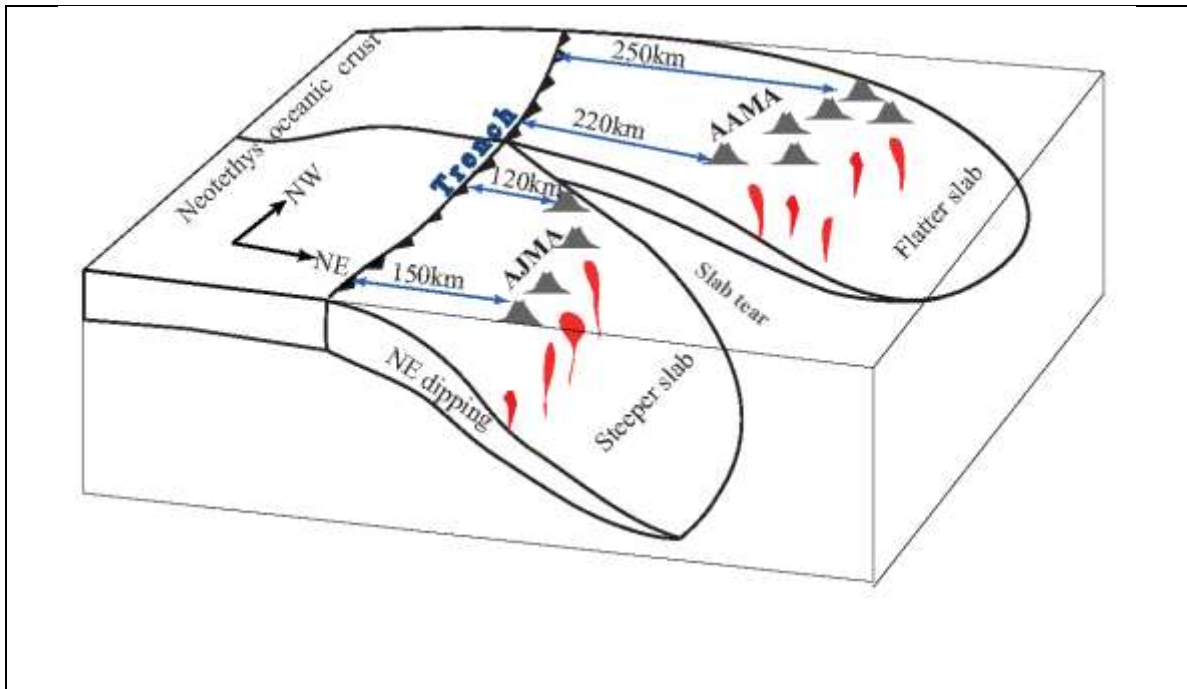


**Figure 10:** Schematic model of the Neo-Thetys ocean paleo-subduction beneath the Iranian plateau based on this study. The model explains the shift in the arc-trench distance with changing angle of subduction according to **Figure 9**.

